DarkSide-20k sensitivity to light dark matter particles

Check for updates

The DarkSide-20k Collaboration*

The dual-phase liquid argon time projection chamber is presently one of the leading technologies to search for dark matter particles with masses below 10 GeV c^{-2}. This was demonstrated by the DarkSide-50 experiment with approximately 50 kg of low-radioactivity liquid argon as target material. The next generation experiment DarkSide-20k, currently under construction, will use 1,000 times more argon and is expected to start operation in 2027. Based on the DarkSide-50 experience, here we assess the DarkSide-20k sensitivity to models predicting light dark matter particles, including Weakly Interacting Massive Particles (WIMPs) and sub-GeV c^{-2} particles interacting with electrons in argon atoms. With one year of data, a sensitivity improvement to dark matter interaction cross-sections by at least one order of magnitude with respect to DarkSide-50 is expected for all these models. A sensitivity to WIMP–nucleon interaction cross-sections below 1×10^{-42} cm^2 is achievable for WIMP masses above 800 MeV c^{-2}. With 10 years exposure, the neutrino fog can be reached for WIMP masses around 5 GeV c^{-2}.

The presence of dark matter (DM) in the universe is supported by many observations based on gravitational effects[1–3] but its real nature remains unknown. Dark matter may consist of an undiscovered elementary particle[4]. A leading candidate is a Weakly Interacting Massive Particle (WIMP), with a mass ranging from 10 GeV c^{-2} to few TeV c^{-2}. This range is extensively searched for via elastic scattering off atomic nuclei—later called nuclear recoils (NR). These searches often use underground Time Projection chambers (TPC)[5–9]. The lack of concrete evidence of direct DM detection so far motivates the search for lighter WIMPs, below 10 GeV c^{-2}, and for light DM candidates interacting with shell electrons—later called electron recoils (ER)—which may subsequently produce sufficiently large ionization signals[10].

DarkSide-20k (DS-20k) is the next generation of liquid argon (LAr) dual-phase TPCs, presently in construction at INFN Laboratori Nazionali del Gran Sasso in Italy. It is expected to start taking data in 2027. It is primarily designed to perform a nearly instrumental background-free search for high mass (>10 GeV c^{-2}) WIMPs. DS-20k aims for <0.1 background events with an exposure of 200 ton · year. The detection mechanism relies on the combined observation of the scintillation light (S1) and ionization (S2) signals. DarkSide-50 (DS-50), a first generation LAr dual-phase TPC, already demonstrated the capability of the technology and obtained world best sensitivities to light DM particles using only the S2 signal, when the S1 signal is no longer observable[11,12]. The analysis was based solely on the number of electrons in S2 (N_{e^-}) as discriminating variable. An update based on the capability to measure the liquid argon ionization yield for low energy electron and nuclear recoils down to $\sim$180 eVer and $\sim$500 eVnr[13], respectively,

was one of the key ingredients to obtain world best limits for WIMPs in the mass range [1.2, 3.6] GeV c^{-2}[14]. A factor of 10 improvement with respect to the previously published limit of Ref. 11 was achieved. The analysis was also used to place limits on DM–nucleon interaction via the Migdal effect[15] and on sub-GeV c^{-2} DM–electron scattering[16]. The stability of the electro-luminescence yield has been measured to be better than 0.5% over almost three years[17]. Based on these successes of DS-50, this article presents the low-mass DM sensitivity prospects for the DS-20k detector. DS-20k will increase the low-radioactivity LAr volume by about a factor of 1,000 with respect to DS-50. It will also significantly improve the radio-purity of the components surrounding the active volume. A detector specifically designed for the investigation of light dark matter using LAr and assuming further isotopic depletion via cryogenic distillation has also been recently studied[18].

Results and discussion

The DS-20k detector

The DS-20k TPC is filled with a 49.7 ton active mass of argon extracted from underground CO_2 wells, hence called Underground Argon (UAr). The TPC is shaped as a prism with an octagonal base, with a vertical drift length of 348 cm and an octagonal inscribed circle diameter of 350 cm. The active volume is immersed in a uniform electric field generated by applying a voltage potential of 73.4 kV between the anode and the cathode made of transparent acrylic (PMMA) coated with a conductive material (Clevios™). The corresponding maximum drift time for the ionization electrons is 3.7 ms. A set of 200 μm wide stainless steel wires spaced by 3 mm located 3 mm below the liquid level is used to define a high field extraction region for

✉e-mail: ds-ed@lists.infn.it; *A list of authors and their affiliations appears at the end of the paper.

drifting electrons. A multiplication region filled with gaseous argon, 7 mm thick between the liquid level and the anode, allows the S2 electroluminescence signal to develop.

To ensure the best possible collection of both scintillation and ionization-induced photons, the inner TPC walls are covered with reflectors. All the inner surfaces are coated with tetraphenyl butadiene to shift the native argon UV light to visible wavelength for which photo-detection efficiency is maximal. Two planes of cryogenic Silicon Photo Multipliers (SiPMs) covering the top and the bottom faces of the TPC detect the light signals. The ~200 k SiPMs are gathered in 5×5 cm^2 arrays, called Photo Detector Modules (PDMs)[19]. PDMs include the front-end electronics[20] and are arranged in 2112 readout channels. The S2 yield is about 25 photoelectrons per ionization electron extracted in the gas pocket. If neutrons scatter in the TPC and produce a WIMP-like signal, they are likely to be captured in the 15 cm thick acrylic TPC walls or endcaps that enclose the SiPM planes, with the latter possibly further doped with Gadolinium. Neutrons captured in this way release γ-rays which are detected in the TPC and/or the 32 ton UAr veto surrounding it, which is read by 480 photo detector channels. The TPC and this UAr veto are housed in a stainless steel (SS) vessel. This SS vessel is immersed in a bath of 650 tons of atmospheric argon (AAr), acting as a shield and an outer veto detector for muons and associated products. The AAr is contained in a ProtoDUNE-like membrane cryostat[21]. DS-20k adopts a triggerless data acquisition system ensuring to save all SiPM signals with close to 100% efficiency for single photo-electrons. Figure 1 shows a cross-section of DS-20k.

Selection

The analysis relies on the strategy successfully put in place for DS-50[14] and adapted to DS-20k. WIMPs are expected to scatter only once in the LAr volume of the TPC. As each particle interaction is associated with a S2 pulse, events with a single S2 pulse are selected. Pulses are required to be isolated from any other S2 pulse preceding or following by >3.7 ms—which corresponds to
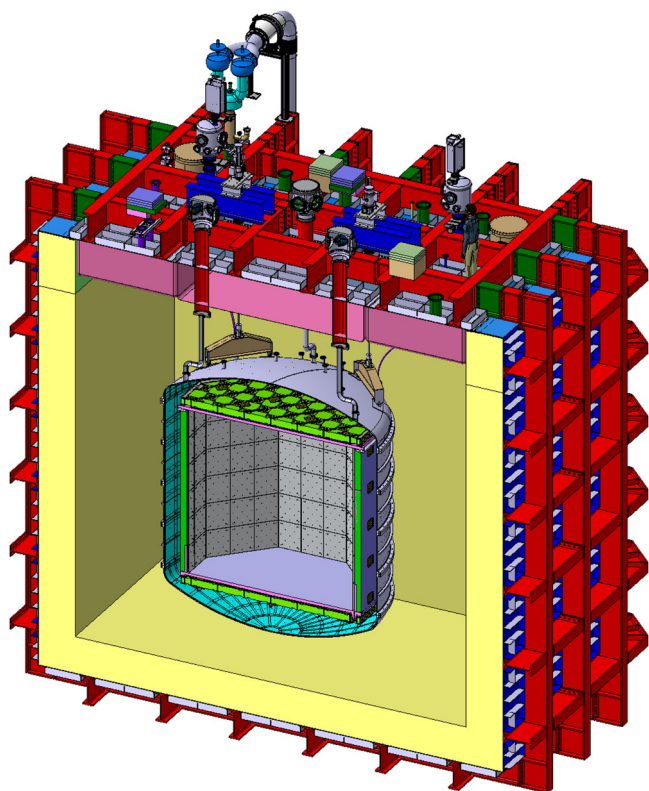

Fig. 1 | Cross-section of the DS-20k detector. The Time Projection Chamber is at the center, with its acrylic walls in green and electrodes in pink. The stainless steel vessel surrounding it is shown in gray, immersed in the ProtoDUNE-like cryostat.

the maximum electron drift time. It is assumed that two close S2 pulses can be distinguished if they are separated in time by >2 μs (2 mm along the drift direction), as achieved in DS-50. Relaxing this assumption produces a negligible impact on the expected sensitivity. Anomalously low S2 could come from α-background. It is assumed that S2 signals can be identified without introducing significant inefficiencies, and that surface α-background that may produce low energy S2 can be efficiently suppressed, as in DS-50. Before any selection procedure, the total rate of ER-events from electron and γ-ray backgrounds from radioactive decays is estimated to be 80 Hz (0.0016 Hz kg^{-1} of UAr) in the TPC, to be compared with 1.5 Hz in DS-50 (0.03 Hz kg^{-1} of UAr). The accidental coincidences within the 3.7 ms isolation window between the S2 pulses induced by this background and by the signal result in an effective livetime of 51%. Unlike the high mass WIMP search analysis, it is not possible to use the pulse shape discrimination of the S1 signal[9,22] to remove the ER background. Instead, the selection aims at mitigating γ-rays and X-rays from radioactive isotopes of the detector components surrounding the UAr active volume (including PDMs). They are efficiently suppressed by a fiducialization based on the S2 pattern in the transverse direction of the TPC, removing an outer 30 cm thick octagonal shell. The position reconstruction resolution along this direction is estimated to be better than 3 cm. As the present analysis is based solely on S2, the drift time, computed as the time difference between S1 and S2, is not available and no fiducialization is performed along the electron drift direction. This procedure leads to a UAr fiducial mass of 34.2 tons, hence an exposure of 17.4 ton · year for one year of data, taking into the account the effective livetime.

Sensitivity results

Using the signal and background models which are thoroughly described in the Methods section, DS-20k prospects for 90% C.L. exclusion limits are derived from a binned profile-likelihood fit implemented in the RooFit package[23]. The likelihood is built as the product of Poissonian terms, one for each of the considered bins. Systematic uncertainties that are believed to be reachable at the time of data taking are accounted for by introducing the nuisance parameters shown in Table 1. They are classified as amplitude or shape systematics, the latter accounting for uncertainties on ^{39}Ar and ^{85}Kr β-decays[14] and on "spurious" electrons (SE) modelling, as well as for spectral distortions from the ionization response.

Figure 2 shows the pre-fit N_{e^-} distribution for the background model. The ^{39}Ar component is dominating for $N_{e^-} \geq 4$. The SE contribution dominates in the $2 \leq N_{e^-} \leq 3$ range and is a factor ~ 18 below ^{39}Ar at $N_{e^-} = 4$. The contribution from the PDMs is dominating the external γ-ray background. The neutrino background from coherent elastic scattering off nucleus (CEνNS) and elastic scattering (ν-ES) off argon electrons is two to four orders of magnitude below the ^{39}Ar background. A typical signal, corresponding to a 2 GeV c^{-2} WIMP mass with a cross-section of 3×10^{-44} cm^2, is superimposed for illustration.

In the following, given the unknowns on the SE background before data taking, two different fit strategies are envisaged: the first one (conservative) is reproducing the DS-50 approach and uses the N_{e^-} range from 4 to 170, while the second one (ultimate) assumes a good understanding of the spurious electrons in DS-20k and uses the total fit range from 2 to 170. Nuisance parameters affecting ^{39}Ar, PDMs, TPC and spurious electrons (only in the ultimate fit case for the latter) are strongly constrained by the fit, since they are related to the dominant backgrounds. For the same reason, a strong (anti-)correlation exists between these amplitude nuisance parameters and the one associated to the exposure. As ^{39}Ar is the dominant background, its spectral shape will need to be computed with higher precision in order to interpret any possible future excess in DS-20k as a signal.

The DS-20k expected median 90% C.L. upper limits on spin-independent WIMP–nucleon cross-section (σ_{SI}), computed with the CLs prescription[24] and for the two fit strategies, are shown in Fig. 3 for 1 year of data. They are compared to the published 90% C.L. limits from DS-50[14] and from other experiments[7,25–31]. An improvement in sensitivity by up to a factor 40 over DS-50 is achieved using the conservative fit. This increases to a

Table 1 | List of systematic uncertainties included in the binned profile likelihood

	Source uncertainty	Affected components
Amplitude	5% on the exposure	All
	15% on ^{39}Ar activity	^{39}Ar
	15% on ^{85}Kr activity	^{85}Kr
	20% on SE normalization	SE
	10% on activity from PDMs	PDMs
	10% on activity from the vessel	Vessel
	10% on activity from the TPC	TPC
	10% on neutrinos normalization	Neutrinos
Shape	atomic exchange and screening	^{39}Ar
	atomic exchange and screening	^{85}Kr
	1% on the ^{39}Ar-decay Q-value	^{39}Ar
	0.4% on the ^{85}Kr-decay Q-value	^{85}Kr
	SE modelling	SE
	ER ionization response	All backgrounds but CEνNS, SE
	NR ionization response	WIMP, CEνNS

Their sources and the impacted signal and background components are indicated, including spurious electrons (SE), external background from Photo Detector Modules (PDMs) and Time Projection chamber (TPC), neutrinos from coherent elastic scattering off nucleus (CEνNS) and Weakly Interacting Massive Particles (WIMP). Any considered spectrum is equally affected by the uncertainty on the dataset exposure, but differs on the ionization response on the basis of the recoil type. The pre-fit uncertainty values are adapted from DS-50 analysis[14].
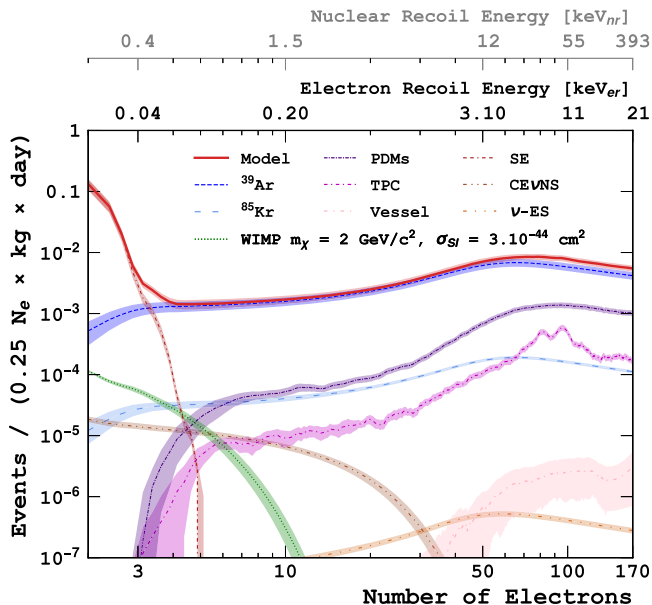

Fig. 2 | Pre-fit DS-20k N_{e^-} spectra distribution. The corresponding ER and NR energy scales are indicated at the top. The pre-fit background model (red line) is shown with its uncertainties (shaded area). Contributions from all the components of the background are also shown. A typical signal model is superimposed for illustration (green dotted line), assuming a 2 GeV c^{-2} WIMP mass with a cross-section of 3×10^{-44} cm^2 and quenching fluctuations.
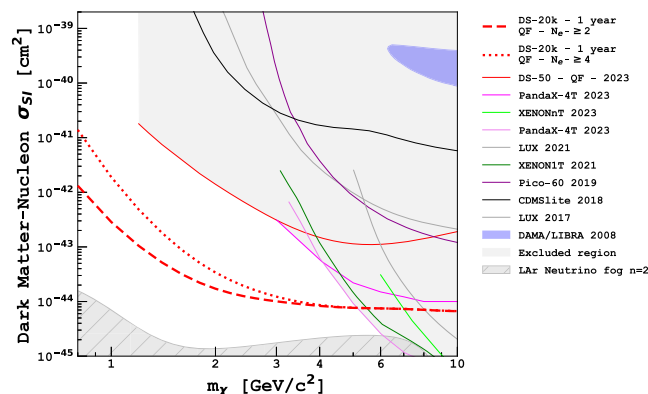

Fig. 3 | Expected DS-20k 90% C.L. exclusion limits for spin-independent WIMP–nucleon cross-section (σ_{SI}). They are shown as bold red lines, assuming quenching fluctuations (QF) (dotted: fit from $N_{e^-} = 4$, dashed: fit from $N_{e^-} = 2$). One year of data is assumed. They are compared to the published 90% C.L. limits from DS-50[14] and from other experiments[7,25–31], with currently excluded parameter space shaded in light gray, as well as claimed discovery from Ref. 49. The neutrino fog in LAr with index $n = 2$[32] is also shown. A local dark matter density of 0.3 GeV c^{-2} cm^{-3} is assumed.

factor 170 at 1.2 GeV c^{-2} WIMP mass with the ultimate fit, reaching a σ_{SI} of 1×10^{-43} cm^2. Overall, a sensitivity to σ_{SI} below 1×10^{-42} cm^2 is achieved for WIMP masses above 800 MeV c^{-2}, covering a large uncharted phase space with 1 year of data. The dominant systematic uncertainties come from the main background (^{39}Ar, SE) modelling and from the detector response (ER ionization yield). The sensitivity would be ~60% better if systematics were neglected. Results without quenching fluctuation on NR are shown in Supplementary Figs. 1 and 2.

The sensitivity scales with the square root of the exposure. With 10 years exposure, the sensitivity will improve by a factor 3 compared to 1 year, whatever the WIMP mass: the neutrino fog in LAr with index $n = 2$[32] could be reached for WIMP masses around 5 GeV c^{-2} (Supplementary Fig. 3).

To assess the robustness of these expectations, variations of detector response model and background activities with respect to the nominal assumptions have been considered. The electron lifetime, single electron response and $x - y$ resolutions and ^{39}Ar activity have been varied by a factor 2 with respect to the nominal assumptions. The main impact comes from the ^{39}Ar activity, assumed to be the same as DS-50, and from the single electron response resolution. If the latter is degraded by a factor 2 with respect to expectations, then the sensitivity would degrade at most by a factor 2 using the ultimate fit strategy, mainly affecting WIMP masses around 1 GeV c^{-2}. A significant improvement in sensitivity is expected if the UAr extraction plant would further reduce the contamination of ^{39}Ar. For a factor 2 lower contamination, the sensitivity would improve up to a factor 1.8 (Supplementary Fig. 4).

The sensitivities to other models described in Refs. 15 and 16 have been evaluated. They are shown in Fig. 4 for 1 year of data, using both conservative and ultimate fit approaches. In both cases and for all models, significant improvements in sensitivity over DS-50 is found over the whole mass ranges, resulting in sensitivity to uncharted phase spaces.

Conclusions

The dual-phase liquid argon time projection chamber is presently one of the leading technologies to search for light galactic dark matter particles with masses below 10 GeV c^{-2}, as demonstrated by the DS-50 experiment with 50 kg of underground liquid argon. Based on this success, a prospect analysis was carried out for the upcoming DS-20k experiment which will have a 1,000 times larger LAr volume target. Already with 1 year of data, a sensitivity improvement to DM–matter interaction cross-sections by at least one order of magnitude with respect to DS-50 is expected for a wide range of DM
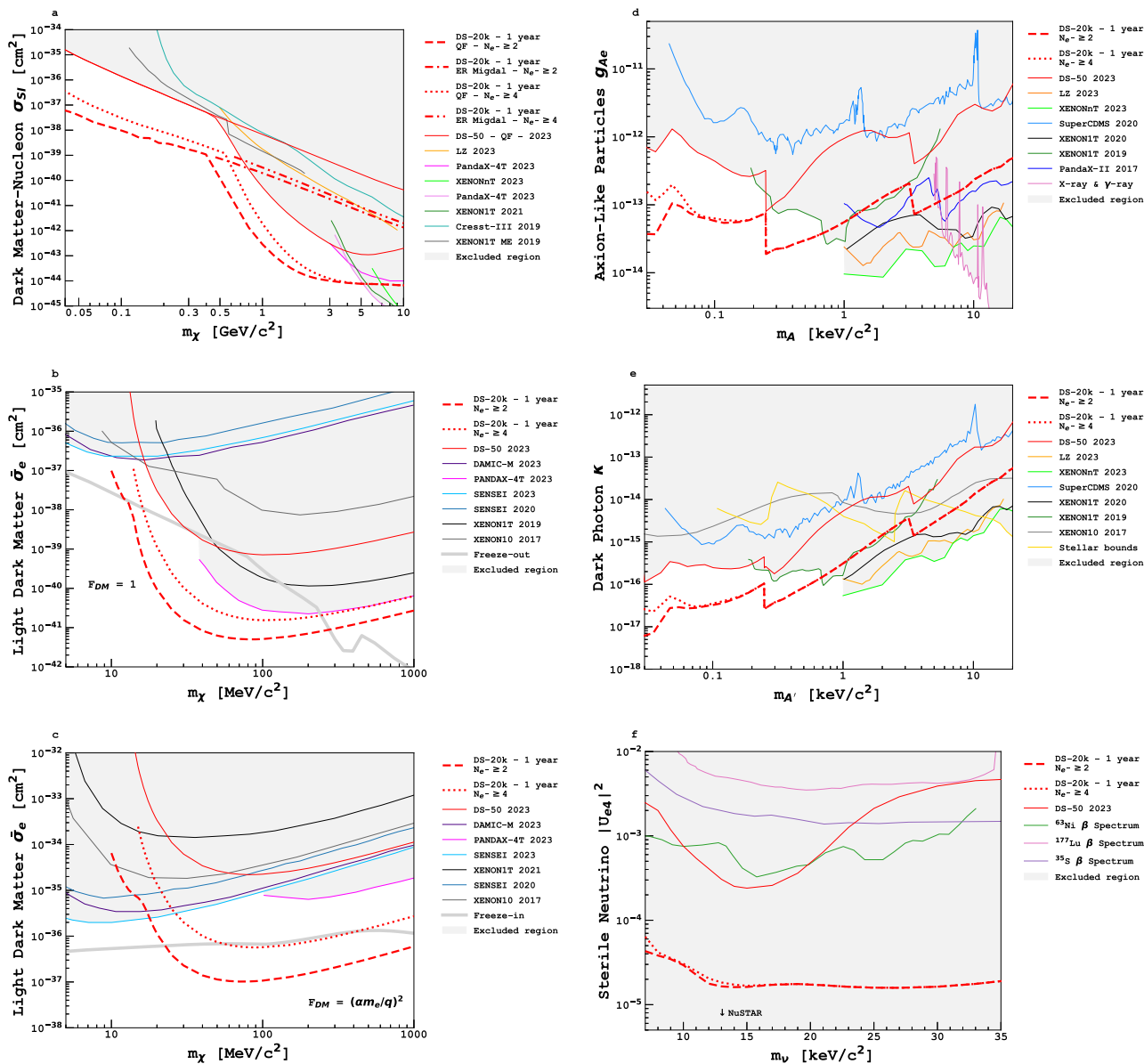
Fig. 4 | Expected DS-20k upper limits at 90% C.L. for various signal models. The *x*-axis shows the mass of the candidate while the *y*-axis shows the model parameter. One year of data is assumed. These results (bold red lines, dotted: fit from $N_{e^-} = 4$, dashed: fit from $N_{e^-} = 2$) are compared to the published 90% C.L. limits from DS-50[15,16], other experiments[7,25–27,50–67] and astrophysical constraints[68–71], with currently excluded parameter space shaded in light gray. **a** Spin-independent WIMP-nucleon cross-section when considering the Migdal effect and with quenching fluctuations (QF) for the NR signal. **b, c** Light dark matter cross-section for an heavy (**b**) and light (**c**) mediator, respectively. Thick lines show cross-sections giving the relic DM

abundance through freeze-in[72,73] or freeze-out[74] production mechanisms. **d** Axion-electron coupling strength g_{Ae}. **e** Kinetic mixing parameter κ between the photon and dark photon. **f** Mixing angle $|U_{e4}|^2$ between sterile neutrino and an active neutrino state. For the latter, the authors of Ref. 16, who contributed to this work as well, identified an error in evaluating the limit, which is corrected here. The indirect detection limits set by the NuSTAR experiment[71], which looks for anomalous X-ray lines from radiative sterile neutrino DM decays, extends downwards to $|U_{e4}|^2 = 10^{-13}$ at 20 keV c^{-2}. A local dark matter density of 0.3 GeV c^{-2} cm^{-3} is assumed.

models: WIMP with or without the Migdal effect in the MeV c^{-2} to GeV c^{-2} mass range as well as Light Dark Matter, axion-like particles, sterile neutrinos and dark photons in the keV c^{-2} or sub-keV c^{-2} mass range. A sensitivity to WIMP–nucleon interaction cross-sections below 1×10^{-42} cm^2 is achievable for WIMP masses above 800 MeV c^{-2}. With 10 years exposure, the neutrino fog in LAr with index $n = 2$ can be reached for WIMP masses around 5 GeV c^{-2}. Further improvements in the sensitivity of DS-20k could be achieved through dedicated measurements aimed at quantifying the fluctuations in quenching for nuclear recoils or identifying the processes underlying the generation of spurious electrons, thereby enabling their effective suppression.

Methods
Detector response model
The number of electrons in S2 is derived from the energy deposited by a single scatter event in the UAr using the ER and NR ionization yields measured by DS-50[13]. The intrinsic fluctuations to ER signals are modelled with an empirical fudge factor implemented as a Fano factor measured by DS-50[13]. Fluctuations from the ionization quenching effect in NR are not known and two models, assuming no fluctuation (NQ) or binomial fluctuations between detectable and undetectable quanta (QF), are considered[14]. Unless explicitly stated, QF is assumed in this article. A Geant4-based Monte Carlo package[33] is used for an accurate simulation of light production,

Table 2 | Estimation of DS-20k material activities for each radio-contaminant, in Bq, for external γ-ray and X-ray background sources

Radio-contaminant	Activity (Bq)		
	TPC	PDMs	SS vessel
^{238}U up	16.1	38.8	21
^{238}U mid	11.5	18.4	8.8
^{238}U low	16.4	449	62
^{232}Th	4.2	17.8	33
^{235}U	0.7	1.8	1.0
^{137}Cs	2.5	2.9	5.0
^{60}Co	2.0	5.1	13
^{40}K	102	269	49

The activity measurements are reported for chain progenitors only, for materials in the Time Projection Chamber (TPC), the Photo Detector Modules (PDMs) and the stainless steel (SS) vessel. In the ^{238}U decay chain, up covers from ^{238}U to ^{222}Rn, mid from ^{222}Rn to ^{210}Pb and low from ^{210}Pb to ^{206}Pb.

propagation and detection for background and signal events. Additionally, effects due to SiPM and electronics noise are simulated on the basis of pre-production SiPM module performance, resulting in a 23% single electron response resolution. Electron losses during the drift due to attachment to impurities are taken into account assuming a 16 ms lifetime, as measured in DS-50[33].

Background model

The β-decay background intrinsic to LAr is fully dominated by the radio-active isotopes ^{39}Ar and ^{85}Kr present in the active volume of UAr. Extracting the argon from underground (same source as DS-50) significantly reduces their contamination with respect to AAr[8]. Their activities are assumed to be 0.73 mBq kg^{-1} and 1.9×10^{-2} mBq kg^{-1}, respectively. The former has the same level as in DS-50 while the latter is reduced by a factor 100 compared to the one of DS-50, thanks to a new multiple distillation column system that has been added at the UAr extraction plant. The argon and krypton spectral shapes are based on calculations of atomic exchange and screening effects, validated on measured ^{63}Ni and ^{241}Pu spectra with a 200 eV threshold[34,35]. Below this value, a linearly increasing uncertainty on the corresponding corrections is assumed, reaching 25% at 0 eV[14]. Further systematics on the spectral shape originate from the uncertainty on the Q-value (1% for ^{39}Ar and 0.4% for ^{85}Kr).

External γ-ray and X-ray backgrounds come from materials used to build the whole inner detector system. Materials are carefully selected for low levels of radioactivity and their activities are measured in an extensive material screening campaign based on the combination of different radio assay techniques. As a summary, Table 2 lists the expected activity of each considered radio-contaminant of the inner detector materials that may lead to γ-ray and X-ray background. Each isotope is simulated uniformly in the component material and decaying particles are tracked over the DS-20k geometry. Thanks to the use of SiPMs instead of classical photomultipliers, the use of PMMA walls for the TPC and the minimization of the amount of passive material, the γ-ray background level is expected to be reduced with respect to DS-50 by a factor 2.5 per surface area orthogonal to the electron drift direction. This validates the extreme care taken to consider radio-pure materials in the design of the DS-20k inner detector.

"Spurious" electrons (SE), whose origin might be ionization electrons trapped by impurities and released later, are a major component of the background at low number of electrons ($N_{e^-} < 4$). The ionization spectrum model is built by fitting DS-50 data in this N_{e^-} range, assuming the same spectrum in DS-20k, with a Poisson distribution convolved with a Gaussian accounting for the single electron response. The origin of the spurious electron signals is assumed to be completely explained by the impurity mechanism in UAr, with the same level of impurities as in DS-50. The expected rate in DS-20k is extrapolated from the DS-50 rate as in Ref. 18.

This background will need to be thoroughly characterized once real DS-20k data is available. The systematic uncertainty on the spectral shape derived from the fit to DS-50 data is assigned to the DS-20k SE modelling.

Other backgrounds to the DM search coming from the interaction of neutrinos via coherent elastic scattering off nucleus (CEνNS)[36], recently observed with argon[37] and xenon[38,39] nuclei, have been considered. The study includes radiative corrections[40] and an accurate parametrization of the nuclear structure[41]. The main contribution impacting this analysis comes from neutrinos from solar ^{8}B which deposit <10 keV in UAr. Elastic scattering (ν-ES) off argon electrons[42] have also been considered, surpassing CEνNS for $N_{e^-} > 30$. In both cases, neutrino fluxes are normalized according to Ref. 43. Finally, the rate of NRs from radiogenic and cosmogenic neutrons is expected to be over four orders of magnitude lower than the ER one, and therefore not considered in this analysis.

Signal models

The signal models are derived assuming the standard isothermal WIMP halo model with an escape velocity of 544 km s^{-1}, a local standard of rest velocity of 238 km s^{-1}, and a local dark matter density of 0.3 GeV c^{-2} cm^{-3}[43]. WIMPs are assumed to elastically scatter off nucleons. Atomic effects predicted by Migdal[44] could add an extra emission of electrons to a fraction of nuclear recoils, increasing the sensitivity to low mass WIMPs. As experimental efforts to confirm the existence of such effects in nuclear scattering are still underway[45–47], WIMP signals with and without them, modelled as in Ref. 15, are considered in this article.

Other dark matter candidates interacting with electrons and producing a S2 signal are possible. First, fermion or scalar boson light dark matter particles with a mass below 1 GeV c^{-2} could interact with bound electrons via a vector mediator. The interaction and cross-section depend on the momentum-transfer q via a form factor F_{DM} and two benchmark models are considered: a heavy mediator with $F_{DM} = 1$ and a light mediator with $F_{DM} = (\alpha m_e / q)^2$ where α is the fine structure constant and m_e the mass of the electron. Other possibilities are the absorption of axion-like particles—coupled to electron via g_{Ae}, and vector-boson like dark photon – mixing with photon via the κ parameter —by argon shell electrons. Finally sterile neutrinos, mixing with an active neutrino state by an angle $|U_{e4}|^2$, could inelastically scatter off a bound electron. All these models are described in details in Ref. 16.

Data availability

The expected limits reported in Figs. 3–4 and Supplementary Figs. 1–3 can be found on Zenodo[48]. The other data that support the findings of this study are available from the corresponding authors upon request.

References

1. Rubin, V. C., Thonnard, N. & Ford Jr, W. K. Rotational properties of 21 SC galaxies with a large range of luminosities and radii, from NGC 4605 /R = 4 kpc/ to UGC 2885 /R = 122 kpc/. *Astrophys. J.* **238**, 471 (1980).
2. Clowe, D. et al. A direct empirical proof of the existence of dark matter. *Astrophys. J. Lett.* **648**, L109–L113 (2006).
3. Aghanim, N. et al. Planck 2018 results. VI. Cosmological parameters. *Astron. Astrophys.* **641**, A6 (2020).
4. Bertone, G., Hooper, D. & Silk, J. Particle dark matter: evidence, candidates and constraints. *Phys. Rept.* **405**, 279–390 (2005).
5. Meng, Y. et al. Dark matter search results from the PandaX-4T commissioning run. *Phys. Rev. Lett.* **127**, 261802 (2021).
6. Aalbers, J. et al. First dark matter search results from the LUX-ZEPLIN (LZ) experiment. *Phys. Rev. Lett.* **131**, 041002 (2023).
7. Aprile, E. et al. First dark matter search with nuclear recoils from the XENONnT experiment. *Phys. Rev. Lett.* **131**, 041003 (2023).
8. Agnes, P. et al. DarkSide-50 532 day dark matter search with low-radioactivity argon. *Phys. Rev. D* **98**, 102006 (2018).

9. Ajaj, R. et al. Search for dark matter with a 231-day exposure of liquid argon using DEAP-3600 at SNOLAB. *Phys. Rev. D* **100**, 022004 (2019).

10. Essig, R., Mardon, J. & Volansky, T. Direct detection of sub-GeV dark matter. *Phys. Rev. D* **85**, 076007 (2012).

11. Agnes, P. et al. Low-mass dark matter search with the DarkSide-50 experiment. *Phys. Rev. Lett.* **121**, 081307 (2018).

12. Agnes, P. et al. Constraints on sub-GeV dark-matter–electron scattering from the DarkSide-50 experiment. *Phys. Rev. Lett.* **121**, 111303 (2018).

13. Agnes, P. et al. Calibration of the liquid argon ionization response to low energy electronic and nuclear recoils with DarkSide-50. *Phys. Rev. D* **104**, 082005 (2021).

14. Agnes, P. et al. Search for low-mass dark matter WIMPs with 12 ton-day exposure of DarkSide-50. *Phys. Rev. D* **107**, 063001 (2023).

15. Agnes, P. et al. Search for dark-matter–mucleon interactions via migdal effect with DarkSide-50. *Phys. Rev. Lett.* **130**, 101001 (2023).

16. Agnes, P. et al. Search for dark matter particle interactions with electron final states with DarkSide-50. *Phys. Rev. Lett.* **130**, 101002 (2023).

17. Agnes, P. et al. Long-term temporal stability of the DarkSide-50 dark matter detector. *JINST* **19**, P05057 (2024).

18. Agnes, P. et al. Sensitivity projections for a dual-phase argon TPC optimized for light dark matter searches through the ionization channel. *Phys. Rev. D* **107**, 112006 (2023).

19. D'Incecco, M. et al. Development of a novel single-channel, 24 cm^2, SiPM-based, cryogenic photodetector. *IEEE Trans. Nucl. Sci.* **65**, 591–596 (2017).

20. D'Incecco, M. et al. Development of a very low-noise cryogenic preamplifier for large-area SiPM devices. *IEEE Trans. Nucl. Sci.* **65**, 1005–1011 (2018).

21. Abi, B. et al. Deep underground neutrino experiment (DUNE), far detector technical design report, volume I introduction to DUNE. *JINST* **15**, T08008 (2020).

22. Amaudruz, P. A. et al. First results from the DEAP-3600 dark matter search with argon at SNOLAB. *Phys. Rev. Lett.* **121**, 071801 (2018).

23. Cranmer, K., Lewis, G., Moneta, L., Shibata, A. & Verkerke, W. *HistFactory: A Tool for Creating Statistical Models for Use With RooFit and RooStats.* http://cds.cern.ch/record/1456844 (2012).

24. Read, A. L. Presentation of search results: the CL(s) technique. *J. Phys. G* **28**, 2693–2704 (2002).

25. Ma, W. et al. Search for solar B8 neutrinos in the PandaX-4T experiment using neutrino-nucleus coherent scattering. *Phys. Rev. Lett.* **130**, 021802 (2023).

26. Li, S. et al. Search for light dark matter with ionization signals in the PandaX-4T experiment. *Phys. Rev. Lett.* **130**, 261001 (2023).

27. Aprile, E. et al. Search for coherent elastic scattering of solar ^{8}B neutrinos in the XENON1T dark matter experiment. *Phys. Rev. Lett.* **126**, 091301 (2021).

28. Akerib, D. S. et al. Improving sensitivity to low-mass dark matter in LUX using a novel electrode background mitigation technique. *Phys. Rev. D* **104**, 012011 (2021).

29. Akerib, D. S. et al. Results from a search for dark matter in the complete LUX exposure. *Phys. Rev. Lett.* **118**, 021303 (2017).

30. Agnese, R. et al. Low-mass dark matter search with CDMSlite. *Phys. Rev. D* **97**, 022002 (2018).

31. Amole, C. et al. Dark matter search results from the complete exposure of the PICO-60 C_3F_8 Bubble Chamber. *Phys. Rev. D* **100**, 022001 (2019).

32. O'Hare, C. A. J. New definition of the neutrino floor for direct dark matter searches. *Phys. Rev. Lett.* **127**, 251802 (2021).

33. Agnes, P. et al. Simulation of argon response and light detection in the DarkSide-50 dual phase TPC. *JINST* **12**, P10015 (2017).

34. Haselschwardt, S. J., Kostensalo, J., Mougeot, X. & Suhonen, J. Improved calculations of beta decay backgrounds to new physics in liquid xenon detectors. *Phys. Rev. C* **102**, 065501 (2020).

35. Mougeot, X. & Bisch, C. Consistent calculation of the screening and exchange effects in allowed β^- transitions. *Phys. Rev. A* **90**, 012501 (2014).

36. Cadeddu, M., Dordei, F. & Giunti, C. A view of coherent elastic neutrino-nucleus scattering. *EPL* **143**, 34001 (2023).

37. Akimov, D. et al. First measurement of coherent elastic neutrino-nucleus scattering on argon. *Phys. Rev. Lett.* **126**, 012002 (2021).

38. Aprile, E. et al. First indication of solar ^{8}B neutrinos via coherent elastic neutrino-nucleus scattering with XENONnT. *Phys. Rev. Lett.* **133**, 191002 (2024).

39. Bo, Z. et al. First indication of solar ^{8}B neutrinos through coherent elastic neutrino-nucleus scattering in PandaX-4T. *Phys. Rev. Lett.* **133**, 191001 (2024).

40. Atzori Corona, M., Cadeddu, M., Cargioli, N., Dordei, F. & Giunti, C. Momentum dependent flavor radiative corrections to the coherent elastic neutrino-nucleus scattering for the neutrino charge-radius determination. *JHEP* **05**, 271 (2024).

41. Cadeddu, M. et al. Physics results from the first COHERENT observation of coherent elastic neutrino-nucleus scattering in argon and their combination with cesium-iodide data. *Phys. Rev. D* **102**, 015030 (2020).

42. Atzori Corona, M. et al. Impact of the Dresden-II and COHERENT neutrino scattering data on neutrino electromagnetic properties and electroweak physics. *JHEP* **09**, 164 (2022).

43. Baxter, D. et al. Recommended conventions for reporting results from direct dark matter searches. *Eur. Phys. J. C* **81**, 907 (2021).

44. Migdal, A. Ionization of atoms accompanying α- and β-decay. *J. Phys. USSR* **4**, 449 (1941).

45. Araújo, H. M. et al. The MIGDAL experiment: measuring a rare atomic process to aid the search for dark matter. *Astropart. Phys.* **151**, 102853 (2023).

46. Xu, J. et al. Search for the migdal effect in liquid xenon with keV-level nuclear recoils. *Phys. Rev. D* **109**, L051101 (2024).

47. Bell, N. F., Dent, J. B., Lang, R. F., Newstead, J. L. & Ritter, A. C. Observing the migdal effect from nuclear recoils of neutral particles with liquid xenon and argon detectors. *Phys. Rev. D* **105**, 096015 (2022).

48. https://zenodo.org/records/13911875.

49. Bernabei, R. et al. Final model independent result of DAMA/LIBRA-phase1. *Eur. Phys. J. C* **73**, 2648 (2013).

50. Aprile, E. et al. Search for light dark matter interactions enhanced by the migdal effect or bremsstrahlung in XENON1T. *Phys. Rev. Lett.* **123**, 241803 (2019).

51. Abdelhameed, A. H. et al. First results from the CRESST-III low-mass dark matter program. *Phys. Rev. D* **100**, 102002 (2019).

52. Barak, L. et al. SENSEI: Direct-detection results on sub-GeV dark matter from a new skipper-CCD. *Phys. Rev. Lett.* **125**, 171802 (2020).

53. Cheng, C. et al. Search for light dark matter-electron scatterings in the PandaX-II experiment. *Phys. Rev. Lett.* **126**, 211803 (2021).

54. Essig, R., Volansky, T. & Yu, T.-T. New constraints and prospects for sub-GeV dark matter scattering off electrons in xenon. *Phys. Rev. D* **96**, 043017 (2017).

55. Aprile, E. et al. Light dark matter search with ionization signals in XENON1T. *Phys. Rev. Lett.* **123**, 251801 (2019).

56. Aprile, E. et al. Emission of single and few electrons in XENON1T and limits on light dark matter. *Phys. Rev. Lett.* **106**, 022001 (2022).

57. Aalbers, J. et al. Search for new physics in low-energy electron recoils from the first LZ exposure. *Phys. Rev. D* **108**, 072006 (2023).

58. Arnquist, I. et al. First constraints from DAMIC-M on sub-GeV dark-matter particles interacting with electrons. *Phys. Rev. Lett.* **130**, 171003 (2023).

59. Adari, P. et al. SENSEI: First direct-detection results on sub-GeV dark matter from SENSEI at SNOLAB. *arXiv* https://doi.org/10.48550/arXiv.2312.13342 (2023).

60. Holzschuh, E., Kundig, W., Palermo, L., Stussi, H. & Wenk, P. Search for heavy neutrinos in the beta spectrum of Ni-63. *Phys. Lett. B* **451**, 247–255 (1999).

61. Mortara, J. L. et al. Evidence against a 17-keV neutrino from S-35 beta decay. *Phys. Rev. Lett.* **70**, 394–397 (1993).

62. Schonert, S. et al. Experimental limits for heavy neutrino admixture deduced from Lu-177 beta decay and constraints on the life time of a radiative neutrino decay mode. *Nucl. Phys. B Proc. Suppl.* **48**, 201–203 (1996).

63. Fu, C. et al. Limits on axion couplings from the first 80 days of data of the PandaX-II experiment. *Phys. Rev. Lett.* **119**, 181806 (2017).

64. Aralis, T. et al. Constraints on dark photons and axionlike particles from the SuperCDMS soudan experiment. *Phys. Rev. D* **101**, 052008 (2020). [Erratum: Phys.Rev.D 103, 039901 (2021)].

65. An, H., Pospelov, M., Pradler, J. & Ritz, A. Direct detection constraints on dark photon dark matter. *Phys. Lett. B* **747**, 331–338 (2015).

66. Aprile, E. et al. Excess electronic recoil events in XENON1T. *Phys. Rev. D* **102**, 072004 (2020).

67. Aprile, E. et al. Search for new physics in electronic recoil data from XENONnT. *Phys. Rev. Lett.* **129**, 161805 (2022).

68. Viaux, N. et al. Neutrino and axion bounds from the globular cluster M5 (NGC 5904). *Phys. Rev. Lett.* **111**, 231301 (2013).

69. Ferreira, R. Z., Marsh, M. C. D. & Müller, E. Do direct detection experiments constrain axionlike particles coupled to electrons? *Phys. Rev. Lett.* **128**, 221302 (2022).

70. An, H., Pospelov, M. & Pradler, J. New stellar constraints on dark photons. *Phys. Lett. B* **725**, 190–195 (2013).

71. Roach, B. M. et al. NuSTAR tests of sterile-neutrino dark matter: new galactic bulge observations and combined impact. *Phys. Rev. D* **101**, 103011 (2020).

72. Bhattiprolu, P. N., McGehee, R. & Pierce, A. Dark sink enhances the direct detection of freeze-in dark matter. *Phys. Rev. D* **110**, L031702 (2024).

73. Boddy, K. K., Freese, K., Montefalcone, G. & Shams Es Haghi, B. Minimal dark matter freeze-in with low reheating temperatures and implications for direct detection. *arXiv* https://doi.org/10.48550/arXiv.2405.06226 (2024).

74. Essig, R. et al. Direct detection of sub-GeV dark matter with semiconductor targets. *JHEP* **05**, 046 (2016).

Author contributions

All authors have contributed to the publication, being variously involved in designing the detector, writing offline software, performing Monte Carlo simulations and data analysis, discussing and approving the scientific results. This article was prepared by a subgroup of authors appointed by the DarkSide Collaboration and subjected to an internal collaboration-wide review process. All authors reviewed and approved the final version of the paper.

Competing interests

D.F. is a Guest Editor for Communications Physics but was not involved in the editorial review of, or the decision to publish this article. All other authors declare no competing interests.

Additional information

Supplementary information The online version contains supplementary material available at https://doi.org/10.1038/s42005-024-01896-z.

Correspondence and requests for materials should be addressed to The DarkSide-20k Collaboration.

Peer review information *Communications Physics* thanks Jelle Aalbers and the other, anonymous, reviewer(s) for their contribution to the peer review of this work. A peer review file is available.

Reprints and permissions information is available at http://www.nature.com/reprints

Publisher's note Springer Nature remains neutral with regard to jurisdictional claims in published maps and institutional affiliations.

The DarkSide-20k Collaboration

F. Acerbi[1], P. Adhikari[2], P. Agnes[3,4], I. Ahmad[5], S. Albergo[6,7], I. F. M. Albuquerque[8], T. Alexander[9], A. K. Alton[10], P. Amaudruz[11], M. Angiolilli[3,4], E. Aprile[12], R. Ardito[13,14], M. Atzori Corona[15,16], D. J. Auty[17], M. Ave[8], I. C. Avetisov[18], O. Azzolini[19], H. O. Back[20], Z. Balmforth[21], A. Barrado Olmedo[22], P. Barrillon[23], G. Batignani[24,25], P. Bhowmick[26], S. Blua[27,28], V. Bocci[29], W. Bonivento[15], B. Bottino[30,31], M. G. Boulay[2], A. Buchowicz[32], S. Bussino[33,34], J. Busto[23], M. Cadeddu[15], M. Cadoni[15,16], R. Calabrese[35], V. Camillo[36], A. Caminata[31], N. Canci[35], A. Capra[11], M. Caravati[3,4], M. Cárdenas-Montes[22], N. Cargioli[15,16], M. Carlini[4], A. Castellani[13,14], P. Castello[15,37], P. Cavalcante[4], S. Cebrian[38], J. M. Cela Ruiz[22], S. Chashin[39], A. Chepurnov[39], L. Cifarelli[40,41], D. Cintas[38], M. Citterio[14], B. Cleveland[42,43], Y. Coadou[23], V. Cocco[15], D. Colaiuda[4,44], E. Conde Vilda[22], L. Consiglio[4], B. S. Costa[8], M. Czubak[45], M. D'Aniello[35,46], S. D'Auria[14,47], M. D. Da Rocha Rolo[27], G. Darbo[31], S. Davini[31], S. De Cecco[29,48], G. De Guido[14,49], G. Dellacasa[27], A. V. Derbin[50], A. Devoto[15,16], F. Di Capua[35,51], A. Di Ludovico[4], L. Di Noto[31], P. Di Stefano[52], L. K. Dias[8], D. Díaz Mairena[22], X. Ding[53], C. Dionisi[29,48], G. Dolganov[54], F. Dordei[15], V. Dronik[55], A. Elersich[56], E. Ellingwood[52], T. Erjavec[56], M. Fernandez Diaz[22], A. Ficorella[1], G. Fiorillo[35,51], P. Franchini[21,57], D. Franco[58], H. Frandini Gatti[59], E. Frolov[60], F. Gabriele[15], D. Gahan[15,16], C. Galbiati[53], G. Galiński[32], G. Gallina[53], G. Gallus[15,37], M. Garbini[41,61], P. Garcia Abia[22], A. Gawdzik[62], A. Gendotti[63], A. Ghisi[13,14], G. K. Giovanetti[64], V. Goicoechea Casanueva[65], A. Gola[1], L. Grandi[66], G. Grauso[35], G. Grilli di Cortona[4], A. Grobov[54], M. Gromov[39], M. Guerzoni[41], M. Gulino[67,68], C. Guo[69], B. R. Hackett[9], A. Hallin[17], A. Hamer[70], M. Haranczyk[45], B. Harrop[53], T. Hessel[58], S. Hill[21], S. Horikawa[4,44], J. Hu[17], F. Hubaut[23], J. Hucker[52], T. Hughes[52], E. V. Hungerford[71], A. Ianni[53], V. Ippolito[29], A. Jamil[53], C. Jillings[42,43], S. Jois[21], P. Kachru[3,4], R. Keloth[36], N. Kemmerich[8], A. Kemp[26], C. L. Kendziora[53], M. Kimura[5], K. Kondo[4,44], G. Korga[21], L. Kotsiopoulou[70], S. Koulosousas[21], A. Kubankin[55], P. Kunzé[3,4], M. Kuss[25], M. Kuźniak[5], M. Kuzwa[5], M. La Commara[35,72], M. Lai[73], E. Le Guirriec[23], E. Leason[21], A. Leoni[4,44], L. Lidey[9], M. Lissia[15], L. Luzzi[22], O. Lychagina[74], O. Macfadyen[21], I. N. Machulin[54,75], S. Manecki[42,43,52], I. Manthos[76,77], L. Mapelli[53], A. Marasciulli[4], S. M. Mari[33,34], C. Mariani[36], J. Maricic[65], M. Martinez[38], C. J. Martoff[9,78], G. Matteucci[35,51], K. Mavrokoridis[59], A. B. McDonald[52], J. Mclaughlin[11,21], S. Merzi[1], A. Messina[29,48], R. Milincic[65], S. Minutoli[31], A. Mitra[79], S. Moioli[14,49], J. Monroe[26], E. Moretti[1], M. Morrocchi[24,25], T. Mroz[45], V. N. Muratova[50], M. Murphy[36], M. Murra[12], C. Muscas[15,37], P. Musico[31], R. Nania[41], M. Nessi[80], G. Nieradka[5], K. Nikolopoulos[76,77], E. Nikoloudaki[58], J. Nowak[57], K. Olchanski[11], A. Oleinik[55], V. Oleynikov[60], P. Organtini[4,53], A. Ortiz de Solórzano[38], M. Pallavicini[30,31], L. Pandola[67], E. Pantic[56], E. Paoloni[24,25], D. Papi[17], G. Pastuszak[32], G. Paternoster[1], A. Peck[73], P. A. Pegoraro[15,37], K. Pelczar[45], L. A. Pellegrini[14,49], R. Perez[8], F. Perotti[13,14], V. Pesudo[22], S. Piacentini[29,48], N. Pino[6,7], G. Plante[12], A. Pocar[81], M. Poehlmann[56], S. Pordes[36], P. Pralavorio[23], D. Price[62], S. Puglia[6,7], M. Queiroga Bazetto[59], F. Ragusa[14,47], Y. Ramachers[79], A. Ramirez[71], S. Ravinthiran[59], M. Razeti[15], A. L. Renshaw[71], M. Rescigno[29], F. Retiere[11], L. P. Rignanese[41], A. Rivetti[27], A. Roberts[59], C. Roberts[62], G. Rogers[76], L. Romero[22], M. Rossi[31], A. Rubbia[63], D. Rudik[35,51,75], M. Sabia[29,48], P. Salomone[29,48], O. Samoylov[74], E. Sandford[62], S. Sanfilippo[67], D. Santone[21], R. Santorelli[22], E. M. Santos[8], C. Savarese[62], E. Scapparone[41], G. Schillaci[67], F. G. Schuckman II[52], G. Scioli[40,41], D. A. Semenov[50], V. Shalamova[73], A. Sheshukov[74], M. Simeone[35,82], P. Skensved[52], M. D. Skorokhvatov[54,75], O. Smirnov[74], T. Smirnova[54], B. Smith[11], A. Sotnikov[74], F. Spadoni[9], M. Spangenberg[79], R. Stefanizzi[15], A. Steri[15,83], V. Stornelli[4,44], S. Stracka[25], S. Sulis[15,37], A. Sung[53], C. Sunny[5], Y. Suvorov[35,51,54], A. M. Szelc[70], O. Taborda[3,4], R. Tartaglia[4], A. Taylor[59], J. Taylor[59], S. Tedesco[27], G. Testera[31], K. Thieme[65], A. Thompson[21], A. Tonazzo[58], S. Torres-Lara[71], A. Tricomi[6,7], E. V. Unzhakov[50], T. J. Vallivilayil[3,4], M. Van Uffelen[23], L. Velazquez-Fernandez[70], T. Viant[63], S. Viel[2], A. Vishneva[74], R. B. Vogelaar[36], J. Vossebeld[59], B. Vyas[2], M. B. Walczak[3,4], Y. Wang[69,84], H. Wang[85], S. Westerdale[73], L. Williams[86], R. Wojaczyński[5], M. Wojcik[87], M. M. Wojcik[45], T. Wright[36], Y. Xie[69,84], C. Yang[69,84], J. Yin[69,84], A. Zabihi[5], P. Zakhary[5], A. Zani[14], Y. Zhang[69], T. Zhu[56], A. Zichichi[40,41], G. Zuzel[45] & M. P. Zykova[18]

[1]Fondazione Bruno Kessler, Povo 38123, Italy. [2]Department of Physics, Carleton University, Ottawa, ON K1S 5B6, Canada. [3]Gran Sasso Science Institute, L'Aquila 67100, Italy. [4]INFN Laboratori Nazionali del Gran Sasso, Assergi (AQ) 67100, Italy. [5]AstroCeNT, Nicolaus Copernicus Astronomical Center of the Polish Academy of Sciences, 00-614 Warsaw, Poland. [6]INFN Catania, Catania 95121, Italy. [7]Università of Catania, Catania 95124, Italy. [8]Instituto de Física, Universidade de São Paulo, São Paulo 05508-090, Brazil. [9]Pacific Northwest National Laboratory, Richland, WA 99352, USA. [10]Physics Department, Augustana University, Sioux Falls, SD 57197, USA. [11]TRIUMF, 4004 Wesbrook Mall, Vancouver, BC V6T 2A3, Canada. [12]Physics Department, Columbia University, New York, NY 10027, USA. [13]Civil and Environmental Engineering Department, Politecnico di Milano, Milano 20133, Italy. [14]INFN Milano, Milano 20133, Italy. [15]INFN Cagliari, Cagliari 09042, Italy. [16]Physics Department, Università degli Studi di Cagliari, Cagliari 09042, Italy. [17]Department of Physics, University of Alberta, Edmonton, AB T6G 2R3, Canada. [18]Mendeleev University of Chemical Technology, Moscow 125047, Russia. [19]INFN Laboratori Nazionali di Legnaro, Legnaro (Padova) 35020, Italy. [20]Savannah River National Laboratory, Jackson, SC 29831, USA. [21]Department of Physics, Royal Holloway University of London, Egham TW20 0EX, UK. [22]CIEMAT, Centro de Investigaciones Energéticas, Medioambientales y Tecnológicas, Madrid 28040, Spain. [23]Centre de Physique des Particules de Marseille, Aix Marseille Univ, CNRS/IN2P3, CPPM, Marseille, France. [24]Physics Department, Università degli Studi di Pisa, Pisa 56127, Italy. [25]INFN Pisa, Pisa 56127, Italy. [26]University of Oxford, Oxford OX1 2JD, United Kingdom. [27]INFN Torino, Torino 10125, Italy. [28]Department of Electronics and Communications, Politecnico di Torino, Torino 10129, Italy. [29]INFN Sezione di Roma, Roma 00185, Italy. [30]Physics Department, Università degli Studi di Genova, Genova 16146, Italy. [31]INFN Genova, Genova 16146, Italy. [32]Institute of Radioelectronics and Multimedia Technology, Warsaw University of Technology, 00-661 Warsaw, Poland. [33]INFN Roma Tre, Roma 00146, Italy. [34]Mathematics and Physics Department, Università degli Studi Roma Tre, Roma 00146, Italy. [35]INFN Napoli, Napoli 80126, Italy. [36]Virginia Tech, Blacksburg, VA 24061, USA. [37]Department of Electrical and Electronic Engineering, Università degli Studi di Cagliari, Cagliari 09123, Italy. [38]Centro de Astropartículas y Física de Altas Energías, Universidad de Zaragoza, Zaragoza 50009, Spain. [39]Skobeltsyn Institute of Nuclear Physics, Lomonosov Moscow State University, Moscow 119234, Russia. [40]Department of Physics and Astronomy, Università degli Studi di Bologna, Bologna 40126, Italy. [41]INFN Bologna, Bologna 40126, Italy. [42]Department of Physics and Astronomy, Laurentian University, Sudbury, ON P3E 2C6, Canada. [43]SNOLAB, Lively, ON P3Y 1N2, Canada. [44]Università degli Studi dell'Aquila, L'Aquila 67100, Italy. [45]M. Smoluchowski Institute of Physics, Jagiellonian

University, 30-348 Krakow, Poland. [46]Department of Structures for Engineering and Architecture, Università degli Studi "Federico II" di Napoli, Napoli 80126, Italy. [47]Physics Department, Università degli Studi di Milano, Milano 20133, Italy. [48]Physics Department, Sapienza Università di Roma, Roma 00185, Italy. [49]Chemistry, Materials and Chemical Engineering Department "G. Natta", Politecnico di Milano, Milano 20133, Italy. [50]Saint Petersburg Nuclear Physics Institute, Gatchina 188350, Russia. [51]Physics Department, Università degli Studi "Federico II" di Napoli, Napoli 80126, Italy. [52]Department of Physics, Engineering Physics and Astronomy, Queen's University, Kingston, ON K7L 3N6, Canada. [53]Physics Department, Princeton University, Princeton, NJ 08544, USA. [54]National Research Centre Kurchatov Institute, Moscow 123182, Russia. [55]Radiation Physics Laboratory, Belgorod National Research University, Belgorod 308007, Russia. [56]Department of Physics, University of California, Davis, CA 95616, USA. [57]Physics Department, Lancaster University, Lancaster LA1 4YB, UK. [58]APC, Université de Paris Cité, CNRS, Astroparticule et Cosmologie, Paris F-75013, France. [59]Department of Physics, University of Liverpool, The Oliver Lodge Laboratory, Liverpool L69 7ZE, UK. [60]Budker Institute of Nuclear Physics, Novosibirsk 630090, Russia. [61]Museo Storico della Fisica e Centro Studi e Ricerche Enrico Fermi, Roma 00184, Italy. [62]Department of Physics and Astronomy, The University of Manchester, Manchester M13 9PL, UK. [63]Institute for Particle Physics, ETH Zürich, Zürich 8093, Switzerland. [64]Williams College, Physics Department, Williamstown, MA 01267, USA. [65]Department of Physics and Astronomy, University of Hawai'i, Honolulu, HI 96822, USA. [66]Department of Physics and Kavli Institute for Cosmological Physics, University of Chicago, Chicago, IL 60637, USA. [67]INFN Laboratori Nazionali del Sud, Catania 95123, Italy. [68]Engineering and Architecture Faculty, Università di Enna Kore, Enna 94100, Italy. [69]Institute of High Energy Physics, Chinese Academy of Sciences, Beijing 100049, China. [70]School of Physics and Astronomy, University of Edinburgh, Edinburgh EH9 3FD, UK. [71]Department of Physics, University of Houston, Houston, TX 77204, USA. [72]Pharmacy Department, Università degli Studi "Federico II" di Napoli, Napoli 80131, Italy. [73]Department of Physics and Astronomy, University of California, Riverside, CA 92507, USA. [74]Joint Institute for Nuclear Research, Dubna 141980, Russia. [75]National Research Nuclear University MEPhI, Moscow 115409, Russia. [76]School of Physics and Astronomy, University of Birmingham, Edgbaston, B15 2TT Birmingham, UK. [77]Institute of Experimental Physics, University of Hamburg, Luruper Chaussee 149, 22761 Hamburg, Germany. [78]Physics Department, Temple University, Philadelphia, PA 19122, USA. [79]University of Warwick, Department of Physics, Coventry CV47AL, UK. [80]Istituto Nazionale di Fisica Nucleare, Roma 00186, Italia. [81]Amherst Center for Fundamental Interactions and Physics Department, University of Massachusetts, Amherst, MA 01003, USA. [82]Chemical, Materials, and Industrial Production Engineering Department, Università degli Studi "Federico II" di Napoli, Napoli 80126, Italy. [83]Department of Mechanical, Chemical, and Materials Engineering, Università degli Studi, Cagliari 09042, Italy. [84]University of Chinese Academy of Sciences, Beijing 100049, China. [85]Physics and Astronomy Department, University of California, Los Angeles, CA 90095, USA. [86]Department of Physics and Engineering, Fort Lewis College, Durango, CO 81301, USA. [87]Institute of Applied Radiation Chemistry, Lodz University of Technology, 93-590 Lodz, Poland.